Published OnlineFirst October 10, 2016; DOI: 10.1158/1078-0432.CCR-16-0702

Personalized Medicine and Imaging

Clinical Cancer Research

Large-scale Radiomic Profiling of Recurrent Glioblastoma Identifies an Imaging Predictor for Stratifying Anti-Angiogenic Treatment Response

Philipp Kickingereder[1], Michael Götz[2], John Muschelli[3], Antje Wick[4], Ulf Neuberger[1], Russell T. Shinohara[5], Martin Sill[6], Martha Nowosielski[7], Heinz-Peter Schlemmer[8], Alexander Radbruch[1,8], Wolfgang Wick[4,9], Martin Bendszus[1], Klaus H. Maier-Hein[2], and David Bonekamp[1,8]

Abstract

Purpose: Antiangiogenic treatment with bevacizumab, a mAb to the VEGF, is the single most widely used therapeutic agent for patients with recurrent glioblastoma. A major challenge is that there are currently no validated biomarkers that can predict treatment outcome. Here we analyze the potential of radiomics, an emerging field of research that aims to utilize the full potential of medical imaging.

Experimental Design: A total of 4,842 quantitative MRI features were automatically extracted and analyzed from the multiparametric tumor of 172 patients (allocated to a discovery and validation set with a 2:1 ratio) with recurrent glioblastoma prior to bevacizumab treatment. Leveraging a high-throughput approach, radiomic features of patients in the discovery set were subjected to a supervised principal component (superpc) analysis to generate a prediction model for stratifying treatment outcome to antiangiogenic therapy by means of both progression-free and overall survival (PFS and OS).

Results: The superpc predictor stratified patients in the discovery set into a low or high risk group for PFS (HR = 1.60; $P = 0.017$) and OS (HR = 2.14; $P < 0.001$) and was successfully validated for patients in the validation set (HR = 1.85, $P = 0.030$ for PFS; HR = 2.60, $P = 0.001$ for OS).

Conclusions: Our radiomic-based superpc signature emerges as a putative imaging biomarker for the identification of patients who may derive the most benefit from antiangiogenic therapy, advances the knowledge in the noninvasive characterization of brain tumors, and stresses the role of radiomics as a novel tool for improving decision support in cancer treatment at low cost. *Clin Cancer Res; 22(23); 5765–71. ©2016 AACR.*

Introduction

Antiangiogenic treatment with bevacizumab, a humanized mAb to the VEGFA, is the single most widely used therapeutic agent for patients with recurrent glioblastoma, a highly vascularized invariably fatal brain tumor (1), accounting for the majority of malignant brain tumors in adults (2). Bevacizumab was approved for the treatment of recurrent glioblastoma by the FDA on the basis of two phase II trials that demonstrated durable radiographic and, more importantly, clinical benefit in many patients (3, 4). Although there is much support for the use of bevacizumab, randomized phase III trials (AVAglio, RTOG-0825, EORTC-26101) conducted to date have failed to show an overall survival benefit for bevacizumab in combination with (radio) chemotherapy (5–7), thus indicating that bevacizumab may not be beneficial in unselected populations of patients with glioblastoma (8)

A major challenge is that there are currently no validated biomarkers that would allow appropriate selection of patients with glioblastoma for whom bevacizumab is most beneficial (8, 9) which is the key to personalized medicine. Much of the discussion has focused on molecular characterization using genomic and transcriptomic technologies (10, 11) and analysis of the AVAglio trial indeed suggested that glioblastoma defined as proneural by molecular subtyping may represent a bevacizumab-responsive subgroup (12). However, there remains an unmet clinical need for easily, ideally noninvasively accessible, surrogate biomarkers able to delineate molecular activity and predict outcome to antiangiogenic treatment (13–15). Recent advances in imaging analysis have allowed noninvasive, three-dimensional and quantitative characterization of neoplastic

[1]Department of Neuroradiology, University of Heidelberg Medical Center, Heidelberg, Germany [2]Medical Image Computing, Division Medical and Biological Informatics, German Cancer Research Center (DKFZ), Heidelberg, Germany [3]Department of Biostatistics, Johns Hopkins Bloomberg School of Public Health, Baltimore, Maryland. [4]Neurology Clinic, University of Heidelberg Medical Center, Heidelberg, Germany. [5]Department of Biostatistics and Epidemiology, Center for Clinical Epidemiology and Biostatistics, Perelman School of Medicine, University of Pennsylvania, Philadelphia, Pennsylvania. [6]Division of Biostatistics, DKFZ, Heidelberg, Germany. [7]Department of Neurology, The Medical University of Innsbruck, Innsbruck, Austria. [8]Department of Radiology, DKFZ, Heidelberg, Germany. [9]Clinical Cooperation Unit Neurooncology, German Cancer Consortium (DKTK), DKFZ, Heidelberg, Germany

Note: Supplementary data for this article are available at Clinical Cancer Research Online (http://clincancerres.aacrjournals.org/).

Corresponding Author: Philipp Kickingereder, Department of Neuroradiology, University of Heidelberg, Im Neuenheimer Feld 400, Heidelberg 69120, Germany. Phone: 49 6221-56-39069; Fax: 49 6221-56-4673; E-mail: philipp.kickingereder@med.uni-heidelberg.de

doi: 10.1158/1078-0432.CCR-16-0702

Published OnlineFirst October 10, 2016; DOI: 10.1158/1078-0432.CCR-16-0702

Translational Relevance

Radiomics applies advanced computational methods to convert medical images into a large number of quantitative descriptors of oncologic tissues. In the current study, we used a high-throughput radiomic approach to automatically extract 4,842 quantitative MRI features in 172 patients with recurrent glioblastoma prior to antiangiogenic therapy and analyze their potential for predicting and stratifying treatment response. Our results (i) reveal that radiomics-based classification with machine learning algorithms allows to identify those patients who may gain the most benefit from antiangiogenic therapy, (ii) advance the knowledge in the noninvasive characterization of brain tumors, and (iii) stress the role of radiomics as a novel tool for improving decision-support in cancer treatment at low cost.

tissue (16, 17) with a great potential for therapy guidance by providing a comprehensive view of the entire tumor, accounting for intratumoral heterogeneity, and unrestricted repeatability during the course of the disease (18).

In the current study, we analyze the potential of radiomics, an emerging field of research that aims to utilize the full potential of medical imaging (16, 17), by automatically extracting and analyzing a total of 4,842 quantitative features from MRI in 172 patients prior to induction of bevacizumab treatment. We hypothesize that the extracted radiomic features can be used to construct distinct subtypes with sufficient power to predict and stratify outcome of patients with recurrent glioblastoma receiving antiangiogenic treatment.

Materials and Methods

Patients

Retrospective data evaluation was approved by the local ethics committee of the University of Heidelberg (ethics approval number: S-320/2012) and informed consent was waived. In total, 172 patients diagnosed with recurrent glioblastoma receiving bevacizumab were included in this study. All patients met the following criteria: (i) pathologically confirmed glioblastoma with recurrence based on MRI in the period of February 2008 and June 2015 (only considering primary glioblastoma), (ii) patients regularly treated for glioblastoma recurrence with bevacizumab (Avastin, Roche; 10 mg/kg of body weight) every 2 weeks per cycle, (iii) availability of MRI studies at baseline prior to the initiation of bevacizumab treatment that included a pre- and postcontrast-enhanced T1-weighted 3D magnetization-prepared rapid acquisition gradient echo (MPRAGE) sequence (subsequently referred to as T1 and cT1) as well as a fluid-attenuated inversion recovery (FLAIR) sequence. Patients were excluded from this study if (i) a repeat surgery was performed prior to the initiation of bevacizumab treatment without measurable contrast enhancement at baseline, or if (ii) the MRI data were of insufficient quality resulting from motion artifacts or poor contrast injection.

Baseline epidemiologic and clinical characteristics of all patients are shown in the Supplementary Data S1. Assessment of response to bevacizumab treatment was performed according to the Response Assessment in Neurooncology (RANO) working group criteria (14, 15, 19). At the time of last assessment (February 2016) 91% of patients (157/172) showed tumor progression and 90% of patients (155/172) had died. Overall survival (OS) was calculated from the initiation of bevacizumab treatment until death or last follow-up. Similarly, progression-free survival (PFS) was calculated from the initiation of bevacizumab treatment until tumor progression.

MR imaging

Images were acquired in the routine clinical workup using a 3 Tesla MR system (Magnetom Verio/Trio TIM, Siemens Healthcare) with a 12-channel head–matrix coil. Sagittal T1-weighted 3D MPRAGE images were acquired (TI = 1,100 ms, TE = 4 ms, TR = 1,710 ms, and FA = 15°, in-plane resolution 0.78 × 0.78 mm, section thickness 1 mm) both before (T1) and after (cT1) administration of a 0.1 mmol/kg dose of gadoterate meglumine (DOTAREM, Guerbet). Axial FLAIR images were acquired with TI = 2,400 ms, TE = 85 ms, TR = 8,500 ms, section thickness = 5 mm, and an interslice gap of 5%.

Image post-processing pipeline

Image registration was performed with the FMRIB software library (FSL, http://fsl.fmrib.ox.ac.uk/fsl/fslwiki/FSL). First, brain voxels were isolated by generating a binary brain mask from the T1-volume using the brain extraction tool (20) and transferred to all other imaging volumes (cT1, FLAIR) for each patient. These image volumes were then registered to the brain extracted T1-volume using the linear image registration tool (21, 22) with a mutual information algorithm and a 6-degree of freedom transformation. T1 subtraction volumes (subT1) were generated by voxel-wise subtraction of the T1 from the cT1 volume. Tumor segmentation was then performed semiautomatically to select the contrast-enhancing (CE) portion of the whole tumor (on the subT1 images) using a region-growing segmentation algorithm implemented in ITK-SNAP (www.itksnap.org; ref. 23), as described previously (Fig. 1; refs. 15, 24).

Next, image intensity normalization was performed to transform arbitrary MR signal intensities into standardized intensity ranges for each imaging modality across all subjects, to generate well-defined inputs for quantitative radiomic feature calculations (Fig. 1; Supplementary Data S2 provides detailed information; ref. 25). For each image volume, eight decompositions were calculated using discrete wavelet transformations which effectively decouple textural information by decomposing the original image in a similar manner as Fourier analysis (detailed information provided in the Supplementary Data S3).

Radiomic features extracted from the CE segmentation masks were calculated automatically with the medical imaging toolkit (MITK, www.mitk.org; ref. 26) and included (i) 17 first-order features (FO) (ii) 9 volume and shape features (VSF), and (iii) 162 texture features (TF; Fig. 1). While VSF were calculated using the segmentation mask, FO and TF were calculated for each modality after intensity normalization and in addition for the corresponding wavelet transformations. The final set then consisted of 179 FO and TF as well 1432 wavelet-derived FO and TF derived from the intensity normalized images for each of the three examined modalities (T1, cT1, FLAIR), and 9 VSF, resulting in a total of 4,842 radiomics features for each patient. Details of the feature extraction algorithms and the individual parameters are found in the Supplementary Data S4.

Published OnlineFirst October 10, 2016; DOI: 10.1158/1078-0432.CCR-16-0702

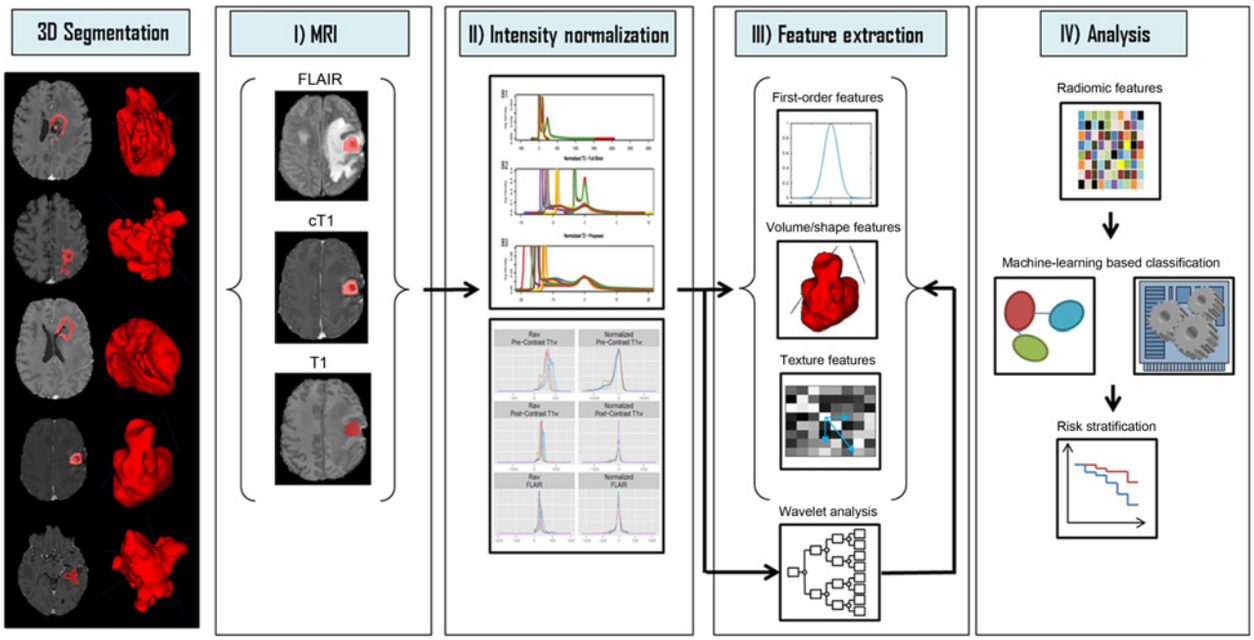

Figure 1.

Image post-processing workflow. Left, different tumors have different shapes and intensities, as shown on representative slices on the left (tumor segmentations in red), with the volume-rendered 3D segmentations on the right. Right, workflow from tumor segmentation to statistical analysis. **I,** three MR imaging sequences [FLAIR, T1 and contrast-enhanced T1 (cT1)] are coregistered to each other. **II,** image intensities are normalized into a common parameter space that allows referencing across different subjects. **III,** multiple radiomic features are automatically calculated from the intensity-normalized images using the 3D segmentations, including first-order, volume/shape, and texture features. In addition, three-dimensional wavelet decomposition is performed on original images and the decomposed images subjected to the same feature extraction routine. **IV,** the large number of radiomic feature parameters is then subjected to supervised principal component analysis, for determination of suitable parameters for survival analyses (for details see text).

Statistical analysis

Subsequent analysis was performed using R version 3.2.3 (R Foundation for Statistical Computing) (27). All radiomic features ($n = 4{,}842$) were normalized by transforming the data into new scores with a mean of 0 and a SD of 1 (z-score transformation). Patients were randomly allocated to a discovery and validation set (2:1 ratio with $n = 112$ patients in the discovery and $n = 60$ patients in the validation set) with the distribution of survival rates kept balanced between both sets.

Next, a supervised principal component (superpc) analysis (with the superpc package (28, 29) implemented in R using default methods and parameters as suggested by the authors) was used to identify a principal component able to stratify treatment outcome (as measured by OS) in the discovery set and then independently validated for patients in the validation set. This technique is similar to conventional principal component analysis except that it uses only a subset of the (radiomic) features that are selected on the basis of their association with the outcome and can be applied to regression and generalized regression problems, such as survival analysis. It compares favorably to other techniques for this type of problem, and can identify which predictor variables are most important (28, 30). Overall, this technique has been shown to allow for robust feature selection and prediction of survival endpoints from high-dimensional data (28, 30–33). Specifically, the discovery set was used to compute coefficients of Cox regression models (Cox scores) for each radiomic feature. Principal components were then calculated on those features with Cox scores exceeding a threshold in absolute value, where the threshold value was estimated by 10-fold cross-validation. Importance scores for the selected radiomic features were calculated equal to their correlation with the first superpc. The first superpc identified in the discovery set was then used to calculate both a continuous and discrete risk score (the latter classified as low or high) for each patient (separately for the discovery and validation set) with the superpc's continuous / discrete prediction model. Finally, cox regression analyses were used to evaluate the performance of the continuous / discrete radiomic superpc predictor for stratifying PFS and OS (separately assessed for both the discovery and validation set). A likelihood ratio test was used to evaluate whether a Cox proportional hazard model that includes the radiomic superpc predictor as explanatory variable significantly improves the model fit as compared with a clinical Cox proportional hazards model [including patients age, interval from initial tumor diagnosis to baseline imaging (prior to bevacizumab treatment), and Karnofsky performance score (KPS) at bevacizumab treatment initiation as explanatory variables] and/or a radiologic Cox proportional hazards model (including contrast-enhancing tumor and edema volumes at baseline imaging prior to bevacizumab treatment as explanatory variables) alone. Furthermore, all parameters (the aforementioned clinical and radiologic parameters as well as the radiomic superpc predictor) were included in a multivariate Cox proportional hazards model to assess the independent significance of the superpc predictor.

Published OnlineFirst October 10, 2016; DOI: 10.1158/1078-0432.CCR-16-0702

The accuracy of the radiomic superpc predictor was assessed as described previously (34–36), by calculating prediction errors over time using the integrated Brier score (IBS; pec package) which can range from 0 for a perfect model to 0.25 for a noninformative model with a 50% incidence of the outcome. Specifically, we generated prediction error curves for Cox proportional hazards models when predicting PFS and OS for patients in the validation set. Cox models have been fitted to the discovery set using the dichotomized risk score from the superpc prediction as explanatory variable. We calculated the IBS of a null model (no explanatory variables, i.e., the marginal Kaplan–Meier estimate) as well as a clinical Cox proportional hazards model and a radiologic Cox proportional hazards model as reference benchmarks. Furthermore, integrated time-dependent AUC curves (iAUC) were calculated for all Cox models by applying the estimator for right-censored time-to-event data proposed by Uno and colleagues (37).

The obtained low- and high-risk groups were assessed for significant differences regarding epidemiologic and clinical characteristics (patient's age, interval from initial diagnosis to bevacizumab treatment, number of recurrences, KPS at treatment initiation), and MGMT promoter methylation status (methylated vs. unmethylated; available for a subset of 60/172 patients) with the Wilcoxon rank-sum and χ^2 test. P values <0.05 were considered significant.

Results

Patients were randomly divided into a discovery and validation set (2:1 ratio) which were balanced for survival (median PFS and OS of 4.8 [95% confidence interval (CI), 3.9–5.5] and 8.6 (95% CI, 6.9–10.2) months for the discovery set and 4.5 (95% CI, 3.1–6.2) and 8.7 (95% CI, 6.8–10.2) months for the validation set; log-rank $P = 0.31$ and 0.75, respectively), as well as for epidemiologic and clinical characteristics [patient's age ($P = 0.67$), KPS ($P = 0.41$), interval initial diagnosis to bevacizumab treatment ($P = 0.78$), and number of recurrences ($P = 0.20$)].

Using the 112 patients (66%) in the discovery set, the superpc analysis identified 72 radiomic features that were most important for predicting treatment outcome using a 10-fold cross-validated threshold. Supplementary Data S5 shows the 72 radiomic features ranked by their importance score for the radiomic superpc predictor. On the basis of these imaging features, the radiomic superpc predictor generated a continuous risk score, which demonstrated a significant association with both PFS [hazard ratio (HR) = 1.74, 95% confidence interval (CI), 1.25–2.41, $P = 0.001$] and OS [HR = 2.13; 95% CI, 1.51–3.00, $P < 0.001$] for patients in the discovery set. The corresponding dichotomized risk score allowed to segment patients into a low- and high-risk group [HR = 1.60 (95% CI, 1.08–2.36) for PFS and 2.14 (95% CI, 1.44–3.19) for OS] with median PFS and OS rates of 5.9 (95% CI, 4.6–8.0) and 11.8 months (95% CI, 9.3–14.5) for the low-risk group, and 3.8 (95% CI, 2.7–4.9) and 6.5 months (95% CI, 4.8–8.4) for the high-risk group (log-rank $P = 0.017$ for PFS and < 0.001 for OS; Fig. 2A and B).

The radiomic superpc predictor trained in the discovery set was then used to predict the treatment outcome in the validation set. Confirming the utility of the radiomic superpc predictor, the estimated continuous risk score for patients in the validation set again demonstrated a significant association with both PFS (HR = 1.76; 95% CI, 1.03–3.00, $P = 0.030$) and OS (HR = 3.48; 95% CI, 1.92–6.28, $P < 0.001$). The corresponding dichotomized risk score again allowed to segment patients into a low- and high-risk group [HR = 1.85 (95% CI, 1.05–3.25) for PFS and 2.60 (95% CI, 1.50–4.51) for OS] with median PFS and OS rates of 5.6 (95% CI, 4.5–12.2) and 11.6 months (95% CI, 9.3–17.7) for the low-risk group, and 2.7 (95% CI, 2.5–5.9) and 6.5 months (95% CI, 4.9–9.5) for the high-risk group (log-rank $P = 0.030$ for PFS and <0.001 for OS; Fig. 2C and D). The radiomic heatmap (Fig. 3) visualizes the 72 features selected by the superpc analysis (separately grouped for discovery vs. validation set and low- vs. high-risk group).

Inclusion of clinical parameters (patients age, initial of initial tumor diagnosis to baseline imaging prior to bevacizumab treatment, KPS at bevacizumab treatment initiation), radiologic parameters (contrast-enhancing tumor and edema volumes at baseline imaging prior to bevacizumab treatment) as well as the superpc predictor as explanatory variables in a multivariate Cox proportional hazards model demonstrated that only the superpc predictor retained independent significance for both PFS ($P < 0.01$) and OS ($P < 0.01$), whereas all other parameters did not (Supplementary Data S6). Furthermore, the likelihood ratio test demonstrated that a Cox proportional hazard model that included the superpc predictor as explanatory variable significantly increased the model fit for both PFS and OS as compared with Cox proportional hazard models that included only the aforementioned clinical and/or radiologic parameters as explanatory variables ($P < 0.01$, respectively).

The predictive accuracy of the radiomic superpc predictor (IBS and iAUC of 0.095 and 0.792 for OS; 0.117 and 0.678 for PFS) was higher as compared Cox proportional hazard models with clinical (IBS and iAUC of 0.106 and 0.704 for OS; 0.128 and 0.541 for PFS) or radiologic parameters (IBS and iAUC of 0.104 and 0.654 for OS; 0.122 and 0.631 for PFS) or a combined model with clinical and radiologic parameters (IBS and iAUC of 0.103 and 0.701 for OS; 0.123 and 0.540 for PFS; Supplementary Data S6). Both scores indicate an improvement in risk prediction with the radiomic superpc predictor.

Finally, correlation between the dichotomized radiomic superpc predictor (i.e., low vs. high risk group) and epidemiologic and clinical characteristics showed that there was no significant difference for age [median, 57 (IQR, 48–63) for the low risk and 55 (IQR, 48–63) for the high-risk groups, $P = 0.81$], KPS [median, 80 (IQR, 70–90) for both groups, $P = 0.12$], number of recurrences [median, 3 (IQR, 1–4) for both groups, $P = 0.57$] or the interval between initial diagnosis and bevacizumab treatment [median, 13.1 months (IQR, 9.4–25.6) for the low risk and 11.0 months (IQR, 8.6–18.2) for the high-risk groups, $P = 0.16$]. Furthermore for the subset of patients with known MGMT status (60/172, 35%) there was no significant difference between MGMT methylated vs. unmethylated tumors and the distribution of the low- and high-risk groups ($P = 0.09$) as well as no significant difference with regard to PFS (log-rank $P = 0.08$) and OS (log-rank $P = 0.27$). Supplementary Data S7 provides information on post-progression therapy after bevacizumab failure.

Discussion

Radiomics applies advanced computational methods to convert medical images into a large number of quantitative descriptors of oncologic tissues (18). In the current study, we used a high-throughput radiomic approach to automatically extract 4,842 quantitative MRI features and analyze their potential

Published OnlineFirst October 10, 2016; DOI: 10.1158/1078-0432.CCR-16-0702

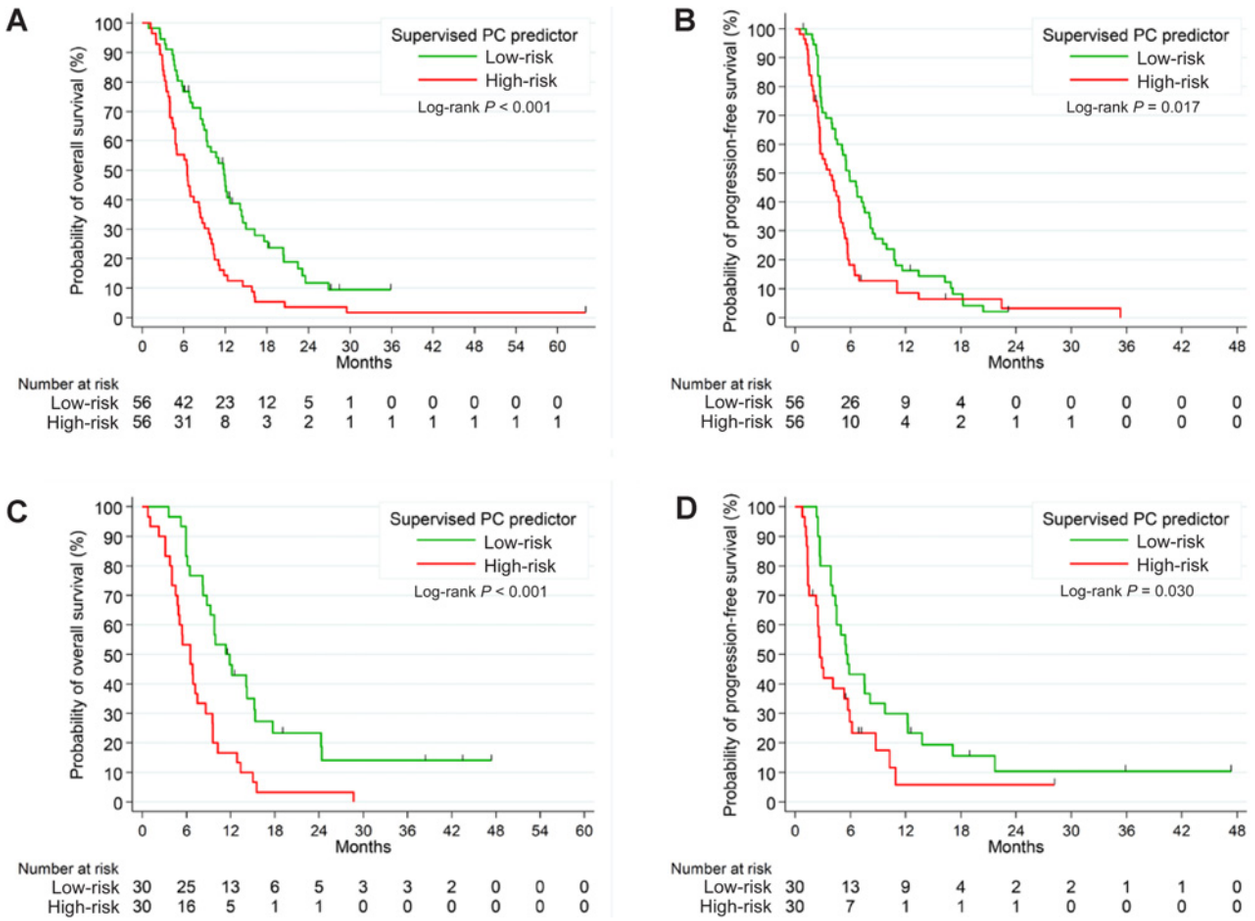

Figure 2.

Kaplan–Meier plot for progression-free and overall survival (PFS, OS) for patients in the discovery (**A, B**) and validation set (**C, D**) stratified by the low- and high-risk group identified by the supervised principal component analysis.

value for stratifying survival of 172 bevacizumab-treated patients with recurrent glioblastoma. Our results reveal that radiomics-based classification of recurrent glioblastoma allows noninvasive survival prediction and stratification of patients with recurrent glioblastoma receiving antiangiogenic treatment, for selecting those patients who may potentially gain the most benefit from antiangiogenic therapy with bevacizumab. Our approach is based on comprehensive quantitative information derived from three different MRI sequences which comprise a multiparametric three-dimensional characterization of the entire tumor, to date undiscovered as a useful source, but also not currently accessible for decision making in clinical practice, owing to the challenges of such an approach. A key challenge for successful implementation of radiomics is the extraction of stable and comparable quantitative image features among different patients as the inherent variability of MRI signal intensities makes direct quantitative analysis difficult; in particular, MRI scans are acquired in arbitrary units that are not comparable between study visits neither within a single patient nor across different patients. To overcome this, we used a novel biologically motivated normalization technique for multisequence MRI (hybrid white stripe normalization) that allows reliable quantitative feature extraction from MRI (25). Next, image features have to be extracted automatically in a high-throughput setting, requiring a substantial amount of computational capacity. Moreover, in radiomics the number of features greatly exceeds the number of patients and conventional regression techniques may produce unsatisfactory results (28). We therefore used a novel superpc analysis, which was shown to be an effective machine-learning algorithm for classification of survival outcomes from high-dimensional data (28, 30–33) to obtain a set of radiomic features that are most important for predicting the outcome of patients receiving antiangiogenic treatment in the discovery set and finally validated the radiomic superpc predictor for patients in the validation set. The corresponding HR for discrimination of PFS and OS based on the superpc's continuous and dichotomized risk score were similar, thus favoring the simplified and clinically more applicable dichotomized (low vs. high) risk score for the selection of patients with recurrent glioblastoma who may derive the most benefit from antiangiogenic therapy.

The clinical relevance of our study lies in the advancement of the noninvasive analysis and characterization of brain tumors, and in the extension of existing knowledge by novel putative

Published OnlineFirst October 10, 2016; DOI: 10.1158/1078-0432.CCR-16-0702

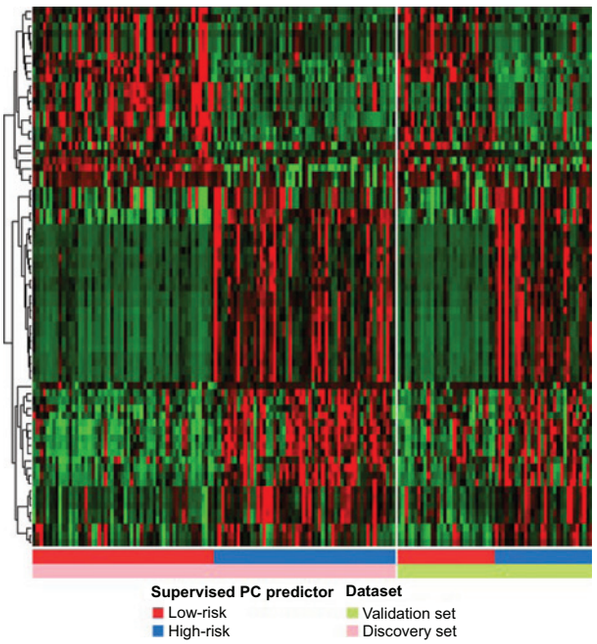

Figure 3.
Heatmap of radiomic features selected by the supervised principal component analysis. Each row corresponds to one z-score normalized radiomic feature, and each column corresponds to one patient (separately grouped for the discovery vs. validation set and low- vs. high-risk group).

imaging biomarkers that currently do not exist in clinical routine. Recent efforts focused on molecular-based response stratification of glioblastoma allocated to antiangiogenic treatment (12, 38, 39) with respect to the four subtypes of glioblastoma established by the Cancer Genome Atlas (TCGA; ref. 10), suggesting benefit for proneural subtypes (12) and lacking benefit for mesenchymal subtypes (12, 38, 39). Despite the importance of these findings, integrative assessment of both molecular and radiomic data may allow to overcome potential shortcomings of a single-sided molecular approach. First, glioblastoma is among the most heterogeneous tumors, and although the different TCGA subtypes reflect the dominant transcriptional program, it may not capture the true diversity of transcriptional subtypes within a tumor, thus emphasizing the clinical significance of intratumoral heterogeneity (40). Second, molecular analysis is usually performed from a single "representative" tumor specimen obtained from surgical debulking or biopsy, which may not account for the molecular heterogeneity between different tumor regions. Taken together, radiomic profiling provides a complementary perspective by making available previously hidden information from MRI (17), which is the imaging modality of choice in brain tumors and routinely performed throughout the disease (19), allowing noninvasive, comprehensive assessment of the complete three-dimensional tumor volume and, by leveraging the results from the current study, emphasizes integrative assessment of both molecular and radiomic data for predicting outcome of patients receiving antiangiogenic treatment.

The most important remaining limitation for the consideration of the described model for guiding treatment decisions is the need for additional confirmatory studies with assessment of a comparative control arm to clarify the value of the radiomic superpc signature as a truly predictive imaging biomarker. Without a bevacizumab-naïve control arm, the treatment-specific predictive value of the model cannot be entirely separated from treatment-independent prognostic factors, although we assessed all available clinical and genetic parameters to assure no obvious bias is present in the data. It is planned to confirm and potentially extend the radiomic signature using data from prospective clinical studies, such as the EORTC 26101 trial (7). Imaging-related limitations may result from the limited through-plane resolution of the FLAIR-data compared with the higher resolution T1-data. As a result, assessment of fine structural detail in one of the three spatial dimensions on the FLAIR-data was affected by some degree of blurring. Furthermore, the sophisticated post-processing workflow involving many steps currently requires about 60 minutes of computation time per patient. With the use of customized high-performance and parallel computing, postprocessing time could, however, be shortened significantly, thus meeting the requirements of translating this technology into clinical practice.

In conclusion, our radiomic-based superpc signature emerges as a putative imaging biomarker for the identification of patients who may derive the most benefit from antiangiogenic therapy, advances the knowledge in the noninvasive characterization of brain tumors, and stresses the role of radiomics as a novel tool for improving decision support in cancer treatment at low cost.

Disclosure of Potential Conflicts of Interest

R.T. Shinohara is a consultant/advisory board member for Genentech, and reports receiving legal consulting fees from Roche. No potential conflicts of interest were disclosed by the other authors.

Disclaimer

The content is solely the responsibility of the authors and does not necessarily represent the official views of the funding agencies.

Authors' Contributions

Conception and design: P. Kickingereder, M. Götz, A. Wick, A. Radbruch, W. Wick, M. Bendszus, K. Maier-Hein, D. Bonekamp
Development of methodology: P. Kickingereder, M. Götz, A. Wick, R.T. Shinohara, K. Maier-Hein, D. Bonekamp
Acquisition of data (provided animals, acquired and managed patients, provided facilities, etc.): P. Kickingereder, A. Wick, M. Nowosielski, A. Radbruch, W. Wick
Analysis and interpretation of data (e.g., statistical analysis, biostatistics, computational analysis): P. Kickingereder, M. Götz, J. Muschelli, A. Wick, U. Neuberger, R.T. Shinohara, M. Sill, W. Wick, M. Bendszus, K. Maier-Hein, D. Bonekamp
Writing, review, and/or revision of the manuscript: P. Kickingereder, M. Götz, J. Muschelli, A. Wick, R.T. Shinohara, M. Sill, M. Nowosielski, H.-P. Schlemmer, A. Radbruch, W. Wick, M. Bendszus, K. Maier-Hein, D. Bonekamp
Administrative, technical, or material support (i.e., reporting or organizing data, constructing databases): P. Kickingereder, A. Wick, U. Neuberger, H.-P. Schlemmer, A. Radbruch, M. Bendszus
Study supervision: P. Kickingereder, M. Bendszus, D. Bonekamp

Grant Support

R.T. Shinohara is funded partially by the NIH under award numbers R01NS085211 and U24CA189523.

The costs of publication of this article were defrayed in part by the payment of page charges. This article must therefore be hereby marked *advertisement* in accordance with 18 U.S.C. Section 1734 solely to indicate this fact.

Received March 17, 2016; revised June 23, 2016; accepted July 7, 2016; published OnlineFirst October 10, 2016.

Published OnlineFirst October 10, 2016; DOI: 10.1158/1078-0432.CCR-16-0702

References

1. Louis DN, Ohgaki H, Wiestler OD, Cavenee WK, Burger PC, Jouvet A, et al. The 2007 WHO classification of tumours of the central nervous system. Acta Neuropathol 2007;114:97–109.
2. Ostrom QT, Gittleman H, Liao P, Rouse C, Chen Y, Dowling J, et al. CBTRUS statistical report: primary brain and central nervous system tumors diagnosed in the united states in 2007–2011. Neuro-Oncol 2014;16:iv1–iv63.
3. Friedman HS, Prados MD, Wen PY, Mikkelsen T, Schiff D, Abrey LE, et al. Bevacizumab alone and in combination with irinotecan in recurrent glioblastoma. J Clin Oncol 2009;27:4733–40.
4. Kreisl TN, Kim L, Moore K, Duic P, Royce C, Stroud I, et al. Phase II trial of single-agent bevacizumab followed by bevacizumab plus irinotecan at tumor progression in recurrent glioblastoma. J Clin Oncol 2009;27:740–5.
5. Chinot OL, Wick W, Mason W, Henriksson R, Saran F, Nishikawa R, et al. Bevacizumab plus radiotherapy-temozolomide for newly diagnosed glioblastoma. N Engl J Med 2014;370:709–22.
6. Gilbert MR, Dignam JJ, Armstrong TS, Wefel JS, Blumenthal DT, Vogelbaum MA, et al. A randomized trial of bevacizumab for newly diagnosed glioblastoma. N Engl J Med 2014;370:699–708.
7. Wick W, Brandes A, Gorlia T, Bendszus M, Sahm F, Taal W, et al. Phase III trial exploring the combination of bevacizumab and lomustine in patients with first recurrence of a glioblastoma: the EORTC 26101 trial [abstract]. In: Proceedings of the 20th Annual Scientific Meeting for the Society for Neuro-Oncology; 2015 Nov 19–22; San, Antonio, TX. Houston (TX): SNO; 2015.
8. Lu-Emerson C, Duda DG, Emblem KE, Taylor JW, Gerstner ER, Loeffler JS, et al. Lessons from anti-vascular endothelial growth factor and anti-vascular endothelial growth factor receptor trials in patients with glioblastoma. J Clin Oncol 2015;33:1197–213.
9. Mayer TM. Can we predict bevacizumab responders in patients with glioblastoma? J Clin Oncol 2015;33:2721–2.
10. Cancer Genome Atlas Research Network, Brat DJ, Verhaak RG, Aldape KD, Yung WK, Salama SR, et al. Comprehensive, integrative genomic analysis of diffuse lower-grade gliomas. N Engl J Med 2015;372:2481–98.
11. Verhaak RG, Hoadley KA, Purdom E, Wang V, Qi Y, Wilkerson MD, et al. Integrated genomic analysis identifies clinically relevant subtypes of glioblastoma characterized by abnormalities in PDGFRA, IDH1, EGFR, and NF1. Cancer Cell 2010;17:98–110.
12. Sandmann T, Bourgon R, Garcia J, Li C, Cloughesy T, Chinot OL, et al. Patients with proneural glioblastoma may derive overall survival benefit from the addition of bevacizumab to first-line radiotherapy and temozolomide: retrospective analysis of the AVAglio Trial. J Clin Oncol 2015;33:2735–44.
13. Nowosielski M, Wiestler B, Goebel G, Hutterer M, Schlemmer HP, Stockhammer G, et al. Progression types after antiangiogenic therapy are related to outcome in recurrent glioblastoma. Neurology 2014;82:1684–92.
14. Kickingereder P, Wiestler B, Burth S, Wick A, Nowosielski M, Heiland S, et al. Relative cerebral blood volume is a potential predictive imaging biomarker of bevacizumab efficacy in recurrent glioblastoma. Neuro Oncol 2015;17:1139–47.
15. Kickingereder P, Radbruch A, Burth S, Wick A, Heiland S, Schlemmer HP, et al. MR perfusion-derived hemodynamic parametric response mapping of bevacizumab efficacy in recurrent glioblastoma. Radiology 2016;279:542–52.
16. Itakura H, Achrol AS, Mitchell LA, Loya JJ, Liu T, Westbroek EM, et al. Magnetic resonance image features identify glioblastoma phenotypic subtypes with distinct molecular pathway activities. Sci Translat Med 2015;7:303ra138.
17. Aerts HJ, Velazquez ER, Leijenaar RT, Parmar C, Grossmann P, Carvalho S, et al. Decoding tumour phenotype by noninvasive imaging using a quantitative radiomics approach. Nat Commun 2014;5:4006.
18. Lambin P, Rios-Velazquez E, Leijenaar R, Carvalho S, van Stiphout RG, Granton P, et al. Radiomics: extracting more information from medical images using advanced feature analysis. Eur J Cancer 2012;48:441–6.
19. Wen PY, Macdonald DR, Reardon DA, Cloughesy TF, Sorensen AG, Galanis E, et al. Updated response assessment criteria for high-grade gliomas: response assessment in neuro-oncology working group. J Clin Oncol 2010;28:1963–72.
20. Smith SM. Fast robust automated brain extraction. Hum Brain Mapp 2002;17:143–55.
21. Jenkinson M, Bannister P, Brady M, Smith S. Improved optimization for the robust and accurate linear registration and motion correction of brain images. NeuroImage 2002;17:825–41.
22. Jenkinson M, Smith S. A global optimisation method for robust affine registration of brain images. Med Image Anal 2001;5:143–56.
23. Yushkevich PA, Piven J, Hazlett HC, Smith RG, Ho S, Gee JC, et al. User-guided 3D active contour segmentation of anatomical structures: significantly improved efficiency and reliability. Neuroimage 2006;31:1116–28. Epub 2006 Mar 20.
24. Bonekamp D, Mouridsen K, Radbruch A, Kurz FT, Eidel O, Wick A, et al. Assessment of tumor oxygenation and its impact on treatment response in bevacizumab-treated recurrent glioblastoma. J Cereb Blood Flow Metab. 2016 Feb 9. [Epub ahead of print].
25. Shinohara RT, Sweeney EM, Goldsmith J, Shiee N, Mateen FJ, Calabresi PA, et al. Statistical normalization techniques for magnetic resonance imaging. Neuroimage Clin 2014;6:9–19.
26. Nolden M, Zelzer S, Seitel A, Wald D, Muller M, Franz AM, et al. The medical imaging interaction toolkit: challenges and advances: 10 years of open-source development. Int J Comp Ass Radiol Surg 2013;8:607–20.
27. R Core Team. R: A Language and Environment for Statistical Computing. Vienna, Austria: R Foundation for Statistical Computing; 2014.
28. Bair E, Tibshirani R. Semi-supervised methods to predict patient survival from gene expression data. PLoS Biol 2004;2:E108.
29. Bair E, Tibshirani R. superpc: supervised principal components; 2012. Available from: http://www-stat.stanford.edu/~tibs/superpc.
30. Bair E, Hastie T, Paul D, Tibshirani R. Prediction by supervised principal components. J Am Stat Assoc 2006;101:119–37.
31. Pellagatti A, Benner A, Mills KI, Cazzola M, Giagounidis A, Perry J, et al. Identification of gene expression-based prognostic markers in the hematopoietic stem cells of patients with myelodysplastic syndromes. J Clin Oncol 2013;31:3557–64.
32. De Cecco L, Bossi P, Locati L, Canevari S, Licitra L. Comprehensive gene expression meta-analysis of head and neck squamous cell carcinoma microarray data defines a robust survival predictor. Ann Oncol 2014;25:1628–35.
33. Chen X, Wang L, Smith JD, Zhang B. Supervised principal component analysis for gene set enrichment of microarray data with continuous or survival outcomes. Bioinformatics 2008;24:2474–81.
34. Gerds TA, Schumacher M. Efron-type measures of prediction error for survival analysis. Biometrics 2007;63:1283–7.
35. Schumacher M, Binder H, Gerds T. Assessment of survival prediction models based on microarray data. Bioinformatics 2007;23:1768–74.
36. Mogensen UB, Ishwaran H, Gerds TA. Evaluating random forests for survival analysis using prediction error curves. J Stat Soft 2012;50:1–23.
37. Uno H, Cai T, Tian L, Wei LJ. Evaluating prediction rules for t-year survivors with censored regression models. J Am Stat Assoc 2007;102:527–37.
38. Sulman EP, Won M, Blumenthal DT, Vogelbaum MA, Colman H, Jenkins RB, et al. Molecular predictors of outcome and response to bevacizumab (BEV) based on analysis of RTOG 0825, a phase III trial comparing chemoradiation (CRT) with and without BEV in patients with newly diagnosed glioblastoma (GBM). J Clin Oncol 31, 2013 (suppl; abstr LBA2010).
39. Piao Y, Liang J, Holmes L, Henry V, Sulman E, de Groot JF. Acquired resistance to anti-VEGF therapy in glioblastoma is associated with a mesenchymal transition. Clin Cancer Res 2013;19:4392–403.
40. Patel AP, Tirosh I, Trombetta JJ, Shalek AK, Gillespie SM, Wakimoto H, et al. Single-cell RNA-seq highlights intratumoral heterogeneity in primary glioblastoma. Science 2014;344:1396–401.

Published OnlineFirst October 10, 2016; DOI: 10.1158/1078-0432.CCR-16-0702

Clinical Cancer Research

Large-scale Radiomic Profiling of Recurrent Glioblastoma Identifies an Imaging Predictor for Stratifying Anti-Angiogenic Treatment Response

Philipp Kickingereder, Michael Götz, John Muschelli, et al.

Clin Cancer Res 2016;22:5765-5771. Published OnlineFirst October 10, 2016.